Asian Journal of Chemistry; Vol. 35, No. 3 (2023), 629-638

ASIAN JOURNAL OF CHEMISTRY

https://doi.org/10.14233/ajchem.2023.27289

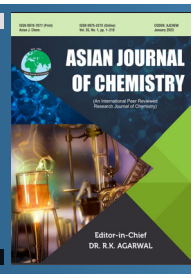

Metanil Yellow Dye Encapsulated Layered Double Hydroxide of Nickel and Aluminium: A Fluorescent and Electrochemical Sensor for Pb^{2+} and Al^{3+} Ion

SAROJMONI KALITA* and DIGANTA KUMAR DAS

Department of Chemistry, Gauhati University, Guwahati, Assam-781003, India

*Corresponding author: E-mail: sarojmoni23@gmail.com

Received: 11 December 2022; *Accepted*: 27 January 2023; *Published online*: 27 February 2023; AJC-21155

In this work, metanil yellow (MY) dye was successfully encapsulated with layered double hydroxide (LDH) of nickel and aluminium was latter synthesized by hydrothermal process. The prepared sensor (MY@NiAl-LDH) was investigated through various characterization techniques. The sensor served as a fluorescent turn-on sensor for Pb^{2+} ion and an electrochemical sensor for Al^{3+} ion. The fluorescent detection of Pb^{2+} is highly selective, reversible with relatively low limit of detection (LOD). It showed fluorescent enhancement mechanism through blocked PET process. Platinum disc electrode modified with MY@NiAl-LDH could selectively detect Al^{3+} ion by cyclic voltammetry in presence of other interfering metal ions. The present work aims to expand dye based layered double hydroxides sensors in the field of feasible detection of biological and environmentally important metal ions.

Keywords: Layered double hydroxide, Turn-on fluorescence sensor, Electrochemical sensor, Cyclic voltammetry.

INTRODUCTION

Heavy metals pollution is a persistent environmental concern and a long-lasting threat to human health and the environment. Lead is one such toxic heavy metals, which is characterized by the low level of degradability, carcinogenicity, high toxicity, bioaccumulation in living organisms and bioavailability [1]. Lead(II) exposure and poisoning can lead to decreased neuronal growth and neurotransmission, loss in memory, loss in focus, kidney damage and failure, genomic instability, *etc.* [2-4]. Although aluminium is stable in its naturally occurring, however, Al^{3+}, one of its ionic forms is known to have neurotoxicological effects such as Alzheimer's disease, Parkinson's disease, osteoporosis, impaired lung function, fibrosis, chronic renal failure, *etc.* [5-7]. Several analytical techniques such as atomic absorption spectroscopy (AAS) [8], inductively coupled plasma emission spectrometry (ICP-AES) [9], electrothermal atomic absorption spectrometry (ETAAS) [10], electroluminescence [11], *etc.* have been used but most of these methods are time consuming, sophisticated and expensive. Among various detection techniques, fluorescence spectroscopy and electrochemical technique has taken over other analytical methods due to its high sensitivity, simplicity, inexpensive operational cost and low detection limit [12].

With the emerging growth of nanostructured materials, layered double hydroxide (LDH)-based sensors have been proven to be a suitable matrix for electrochemical and analytical detection of heavy metals. Layered double hydroxides (LDH) have emerged as a large group of nanomaterials with the general formula $[M^{II}_{1-x}M^{III}_{x}(OH)_2]^{x+}$ $(A^{n-})_{x/n}\cdot mH_2O$, where M^{II} and M^{III} are di- and trivalent metal cations, occupying the octahedral holes of brucite-like layers to form a lamellar structure, respectively and (A^{n-}) is the interlayer charge-balancing anion [13]. A large variety of macromolecules and dye molecules can be intercalated into the interlayer spaces of the LDH by a simple anion-exchange procedure. The ordered structure, surface charges and excellent exchange capacity of LDH can provide stability to anionic dyes from sunlight and high temperature degradation and photo-oxidation [14]. Amini *et al.* [15] reported a hexacyanoferrate intercalated LDH nanozyme for the determination of chromium. In another study, Senda *et al.* [16] prepared Schiff base-intercalated LDHs for selective copper(II) ion capture. An electrochemical sensor based on EDTA intercalated into LDHs of magnesium and aluminum for ultra trace level detection of lead(II) was reported by Dong *et al.* [17]. In another resported work, Liu *et al.* [18] investigated acridine orange dye encapsulated LDH as a potential sensor for detection of Hg(II) ion in water.

Herein, metanil yellow dye (MY) loaded into the matrix of NiAl-LDH (MY@NiAl-LDH) acts a fluorescent "off-on" sensor for Pb^{2+} ions and an electrochemical sensor for detection of Al^{3+} ions. The new sensor exhibits excellent selectivity, reversibility and sensitivity as a fluorescent sensor for Pb^{2+} ions with low detection limits. The metal interference study showed no intereference from other metal ions in the fluorescent detection of Pb^{2+} ions. Platinum disc electrode modified with MY@NiAl-LDH sensor could selectively detect Al^{3+} ions by cyclic voltammetry technique with low detection limit and no interference from other metal ions.

EXPERIMENTAL

All chemicals were purchased either from Sigma Aldrich or LOBA. The metal salts used for spectroscopic measurements except for $Pb(NO_3)_2$, $CdCl_2$ and $HgCl_2$ were sulphates. The chemicals were of analytical grade and used without further purification. The chemical solutions (10^{-3} M) were prepared in deionized water obtained from quartz double-distilled plant and dissolved in phosphate buffer (pH 7.4). The FT-IR spectra were recorded in a Perkin-Elmer RXI spectrometer as KBr pellets. The fluorescence and UV-visible spectra were recorded in HITACHI 2500 and Shimadzu UV 1800 spectrophotometer respectively using quartz cuvette (1 cm path length). The electrochemical measurements were carried out on a CHI660DCH Instrument electrochemical analyzer (USA) consisting of a three-electrode system: Pt electrode as working electrode, Ag/AgCl (3 M NaCl) as auxiliary electrode, Pt wire as reference electrode and KCl as a supporting electrolyte. Scanning electron microscopy was done using Zeiss FESEM Sigma 300 and energy dispersive X-ray spectroscopy was studied using Ametek EDAX. The diffuse reflectance spectra of the samples were recorded in a HITACHI, U-4100 spectrophotometer. Thermogravimetric analysis (TGA) was done using Metter Toledo TGA/DSC1 STAR^e system in presence of N_2 atmosphere in the temperature range 50-700 ºC at a heating rate of 10 ºC/min. Powder X-ray diffraction (PXRD) patterns of the synthesized samples were recorded using a Rigaku Ultima IV X-Ray diffractometer (Cu*K*α radiation, λ = 1.5418 Å) at 40 kV and 40 mA.

Synthesis of NiAl-layered double hydroxide: The NiAl-layered double hydroxide was prepared as reported method [19]. In brief, a mixture of $Ni(NO_3)_2{\cdot}6H_2O$ (3.48 g) and $Al(NO_3)_3{\cdot}9H_2O$ (1.5 g) was dissolved in 40 mL deionized water and subjected to stirring to form a clear solution. To a mixture, 0.4 M NaOH and 0.2 M Na_2CO_3 were added dropwise under continuous stirring to obtain a pH value of 9.6. The suspension was transferred to a 100 mL Teflon-lined stainless steel autoclave. The autoclave was tightly sealed and heated at 180 ºC for 15 h. The resulting light greenish suspension was filtered and washed with deionized water and ethanol. The resulting precipitate was oven-dried at 180 ºC for 12 h followed by calcination at 1000 ºC for 2 h.

Encapsulation of metanil yellow dye loaded NiAl-LDH: The encapsulation of metanil yellow dye into NiAl-LDH was done as per reported method [19]. In brief, the synthesized LDH (2 g) was sonicated in 70 mL deionized water for 0.5 h, to which 0.5 g of metanil yellow dye was added followed by continuous stiring for 24 h. The resulting solution was centrifuged, washed with deionized water and oven dried at 100 ºC for 8 h (**Scheme-I**).

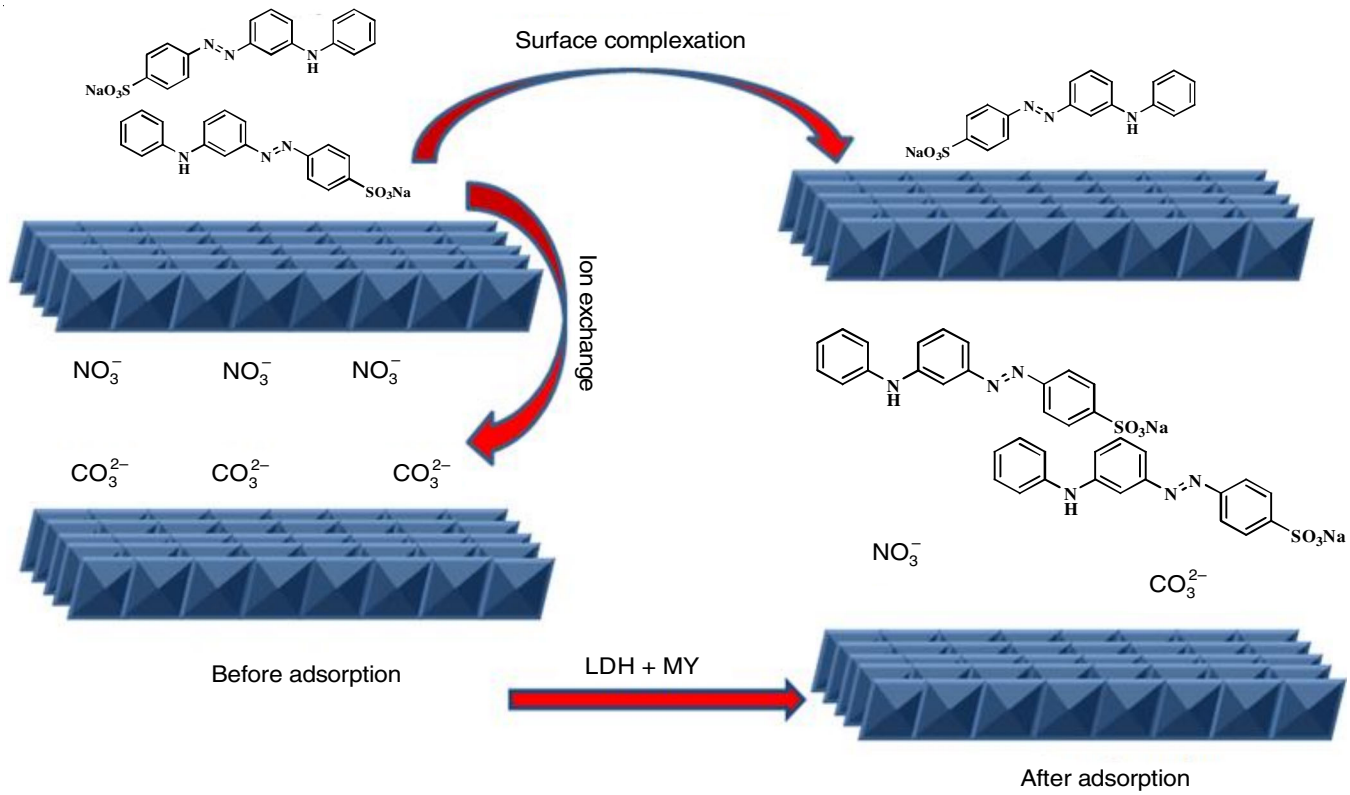

Scheme-I: Synthetic route of metanil yellow (MY) dye encapsulated with layered double hydroxide of nickel and aluminium (MY@NiAl-LDH)

RESULTS AND DISCUSSION

Infrared studies: The FTIR spectra of NiAl-layered double hydroxide and metanil yellow dye intercalated NiAl-layered double hydroxide are shown in Fig. 1. The broad bands around 3500-3400 cm^{-1} are due to the stretching vibrations of the structural O-H groups in LDH and a sharp peak at 1640 cm^{-1} can be prescribed to the bending vibration of the interlayer water molecules. Bands in the region around 800-500 cm^{-1} can be related to the metal-oxygen and metal-hydroxyl bending vibrations, respectively. Moreover, sharp peaks at 1383 cm^{-1} and 1549 cm^{-1} can be attributed to the stretching modes of NO_3^- and CO_3^{2-} groups in the interlayer of LDHs. After the encapsulation of dye into LDH, the intensity of the peak corresponding to NO_3^- decreases and several new peaks appear. Metanil yellow loaded LDH shows peaks at 1625 cm^{-1} due to C=C stretching mode of benzene ring, 1213 cm^{-1} due to the C-N stretching vibration, the azo group peak appears at 1490 cm^{-1} and the SO_3^{2-} asymmetric stretching and bending mode peak appears at 1250 cm^{-1} and 640 cm^{-1}, respectively.

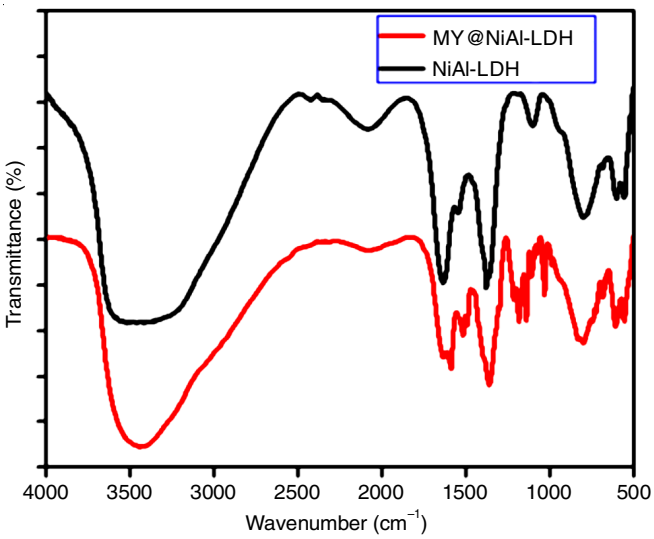

Fig. 1. FTIR spectrum of NiAl-LDH and MY@NiAl-LDH

PXRD studies: The PXRD pattern of NiAl-LDH showed peaks corresponding to symmetric reflections for (003), (006), (110) and (113) planes and broad asymmetric peaks for (009), (015) and (018) planes, respectively (Fig. 2). These results indicated that the synthesized LDH has a well-ordered layered crystalline structure (space group $R\bar{3}m$). The dye loaded LDH demonstrated some broadening of fundamental peaks. Also, after encapsulation of the dye into the pristine LDH, the basal spacing d value corresponding to (003) reflection has increased from 7.49 to 9.25 Å.

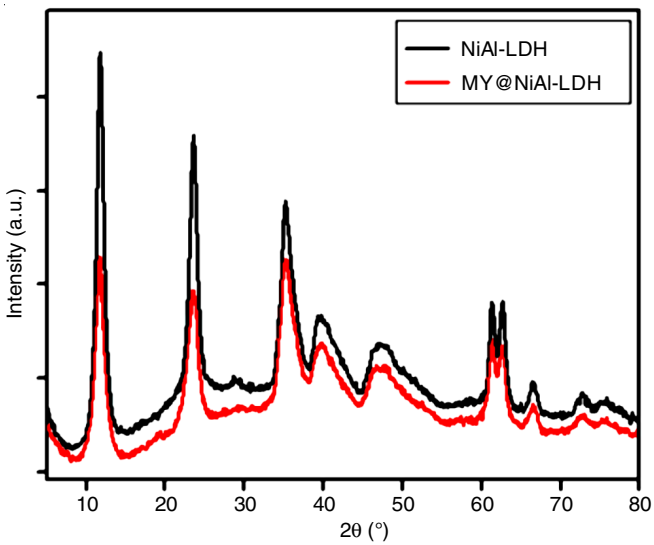

Fig. 2. PXRD patterns of NiAl-LDH and MY@NiAl-LDH

SEM and EDAX studies: The SEM image of pure NiAl-LDH has irregular shaped flake-like morphology stacked by a large number of platelet-like units with rough surfaces (Fig. 3a). After encapsulation with the dye, the morphology slightly changes as the nanoflakes exhibited rougher edges with more aggregation (Fig. 3b). Moreover, some particles appeared on the surface are mainly due to the adsorption of metanil yellow dye. The EDAX profile of pure LDH and dye loaded LDH shows the elemental presence of Ni, Al, O and Ni, Al, O, C, N, S, respectively (Fig. 4), whereas the elemental mapping of the nanosensor is depicted in Fig. 5.

UV-Vis/diffuse reflectance spectra: Fig. 6 shows the diffuse reflectance spectrum of NiAl-LDH in which five absorption

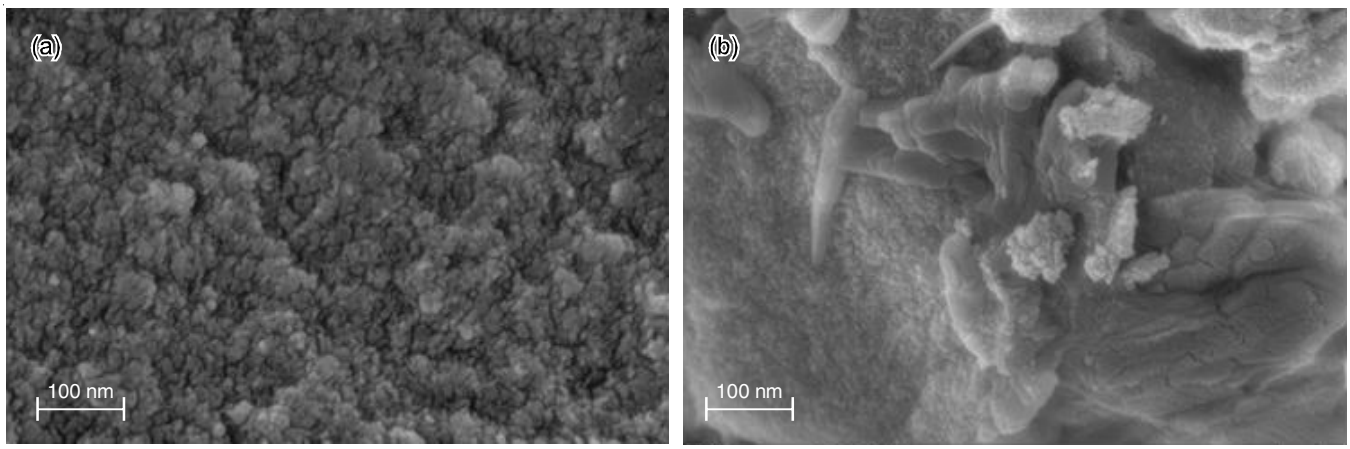

Fig. 3. SEM images of (a) NiAl-LDH and (b) MY@NiAl-LDH

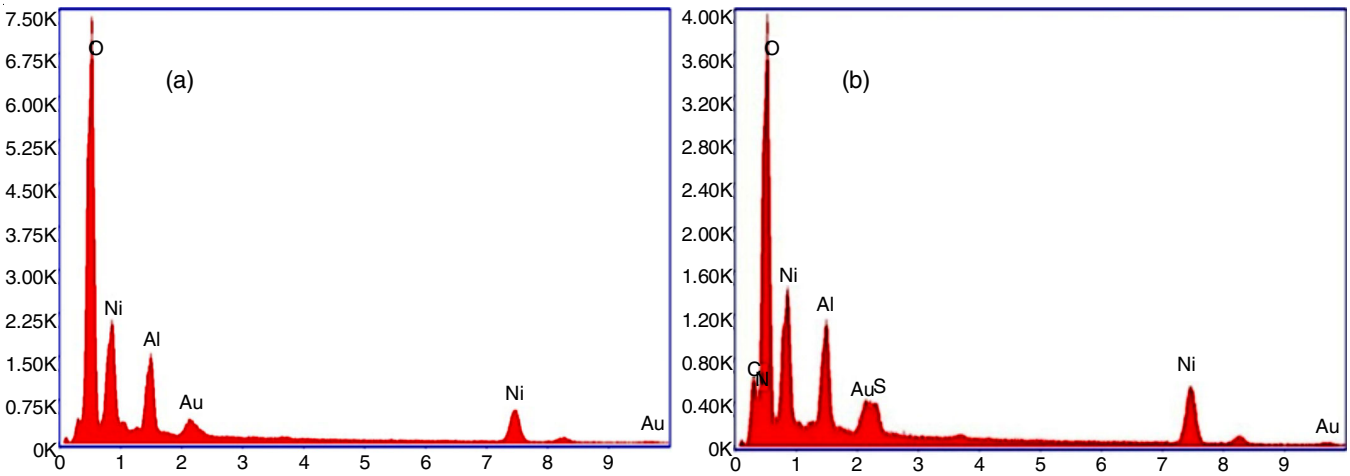

Fig. 4. EDAX spectra of (a) NiAl-LDH and (b) MY@NiAl-LDH

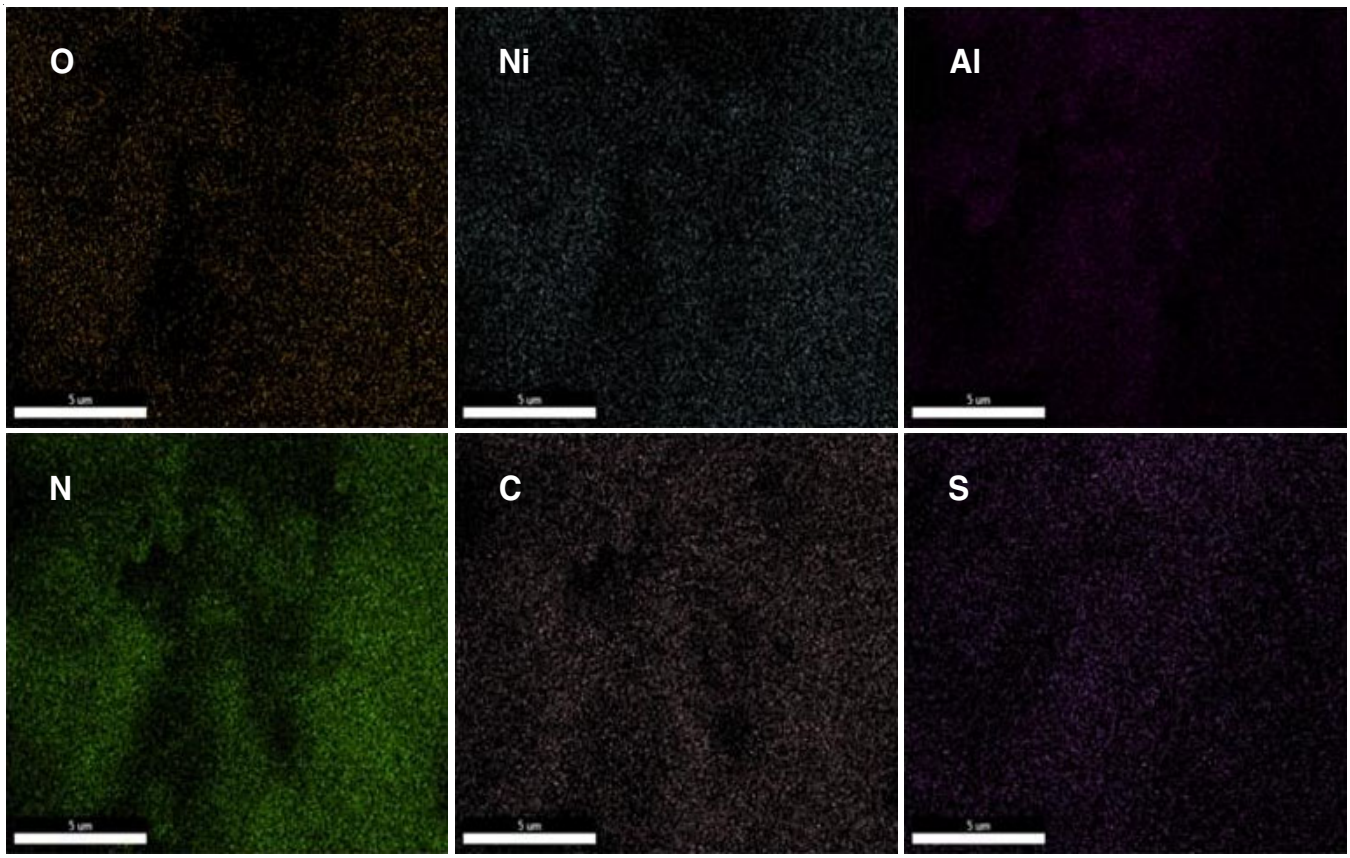

Fig. 5. Elemental mapping of MY@NiAl-LDH

peaks appear at 205, 377, 415, 645 and 1105 nm, respectively. The peak corresponding to 205 and 377 nm can be attributed to the charge transfer transitions originating from a transition from oxygen to Ni^{2+} and Al^{3+} of LDH moiety. The peak at 415 and 645 nm can be assigned to the $3A_{2g} \rightarrow {}^3T_{1g}(F)$ and ${}^3A_{2g} \rightarrow {}^3T_{1g}(P)$ transitions of octahedral Ni-hydroxo complex in the LDH. After the loading of dye into the LDH, the higher energy bands suffer a blue shift whereas the lower energy bands are found to be shifted into the red region.

Thermal studies: In thermogravimetric analysis of NiAl-LDH (Fig. 7), the first weight loss at around 60-120 ºC is due to the loss of interlayer water molecules. The second weight loss around 230-290 ºC is attributed to dehydroxylation and the final weight loss in the range of 320-450 ºC is due to the decomposition of interlayer ions in the LDH. In case of dye intercalated LDH, the first weight loss in the temperature range of 50-150 ºC arises due to loss of surface adsorbed and interlayer water molecules. The second mass loss in the range of 160-260 ºC occured due to the decarboxylation and dehydroxylation in the hybrid material. The third weight loss in the range of 280-460 ºC is ascribed to the hydrocarbon loss of aromatic moiety of the dye molecule and breakage of the dye

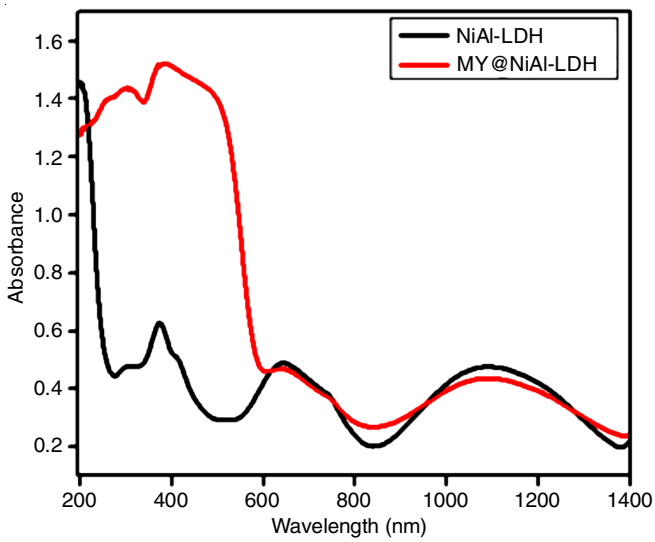

Fig. 6. UV-Vis/DRS spectra of NiAl-LDH and MY@NiAl-LDH

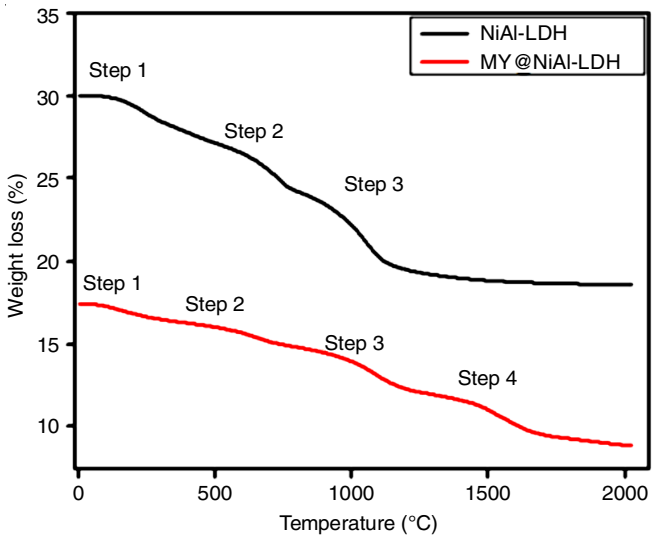

Fig. 7. Thermogram curve of NiAl-LDH and MY@NiAl-LDH

linkages. The last mass loss at a slightly higher temperature can be attributed to the loss of sulphate anions in dye molecule and stable combustion of the encapsulated metanil yellow dye.

MY@NiAl-LDH as fluorescent sensor for Pb^{2+}: The MY@NiAl-LDH (0.01 g) was dispersed in 5 mL methanol and sonicated for 10 min to get a fine dispersion. A 10^{-3} M metal salt solutions were prepared in a double-distilled water using quartz double-distilled plant in phosphate buffer solution (pH = 7.4). From the UV-Vis spectrum, the excitation wavelength for the sensor was fixed at 275 nm. The fluorescence spectrum of MY@NiAl-LDH in CH_3OH/PBS buffer (1:1, pH = 7.4) was recorded in a quartz cuvette of path length 1 cm and the solution was irradiated with 275 nm of photons. The emission range was kept constant within the range 275-600 nm wherein two fluorescence peaks of intensity *ca.* 101 and 79 were observed at λ_{max}= 344 nm and 375 nm. A 100 µL of different metal solutions (10^{-3} M) was added one at a time into the cuvette containing a solution of MY@NiAl-LDH and its fluorescent spectrum was recorded. The fluorescence intensity increased only in case of Pb^{2+} and Al^{3+}, however, an increment of intensity in case of Al^{3+} is not gradual. The I/I_0 values of MY@NiAl-LDH in presence of one equivalent of different metal ions is shown in Fig. 8, where I is the fluorescent intensity of MY@NiAl-LDH on addition of a particular metal ion and I_o is the fluorescent intensity of MY@NiAl-LDH in absence of any metal ions. It can be inferred from the plot that only Pb^{2+} increases the intensity of MY@NiAl-LDH to a considerable extent.

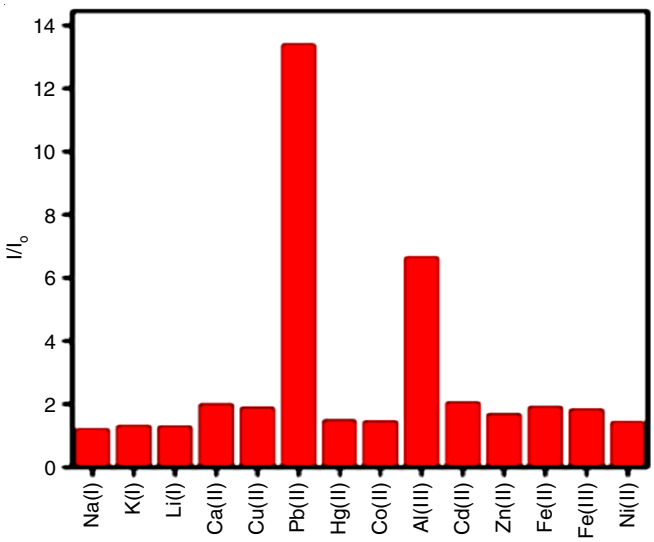

Fig. 8. The I/I_0 value of MY@NiAl-LDH in CH_3OH/PBS buffer (1:1, pH = 7.4) in presence of different ions

Fig. 9 shows the gradual enhancement in fluorescence intensity of MY@NiAl-LDH on the addition of different concentrations of Pb^{2+}. The peak at 375 nm disappears and the peak at 344 nm gradually increases upon addition of Pb^{2+} solution. The final enhancement of peak intensity MY@NiAl-LDH is about 13 times the initial intensity upon addition of 20 equivalents of Pb^{2+} (0-200 µL). The plot of fluorescence intensity with respect to the analyte concentration fits linearly with R^2 = 0.989 (Inset, Fig. 9b). The stoichiometry of binding and the binding constant for the interaction of MY@NiAl-LDH with Pb^{2+} was calculated from the plot of log $[(I_0\text{-}I)/(I\text{-}I_{max})]$ *versus* $[Pb^{2+}]$ [20]. Here, I_0 is the fluorescence intensity of MY@NiAl-LDH in absence of Pb^{2+}; I is the fluorescence intensity of MY@NiAl-LDH at different added concentrations of Pb^{2+} and I_{max} is the highest intensity of MY@NiAl-LDH upon titration with Pb^{2+}. The slope of the plot and R^2 was found to be 1.372 and 0.994 respectively (Fig. 10). The value of the slope indicates a 1:1 interaction between MY@NiAl-LDH and Pb^{2+} and the binding constant was found to be log $\beta = 10^{4.8}$. The limit of detection (LOD) was calculated using the formula: $3\sigma/K$ [21], where σ = standard deviation, K = slope obtained from the plot of fluorescence intensity *vs.* concentration of Pb^{2+}. The LOD was found to be 0.405 nM. A comparison of MY@NiAl-LDH sensor with some other reported sensors with their LOD's for Pb^{2+} is displayed in Table-1.

Absorption studies: The UV-vis spectra of MY@NiAl-LDH showed two peaks at 275 and 425 nm, respectively. On titrating with gradual addition of Pb^{2+} ion, the peak at 425 nm

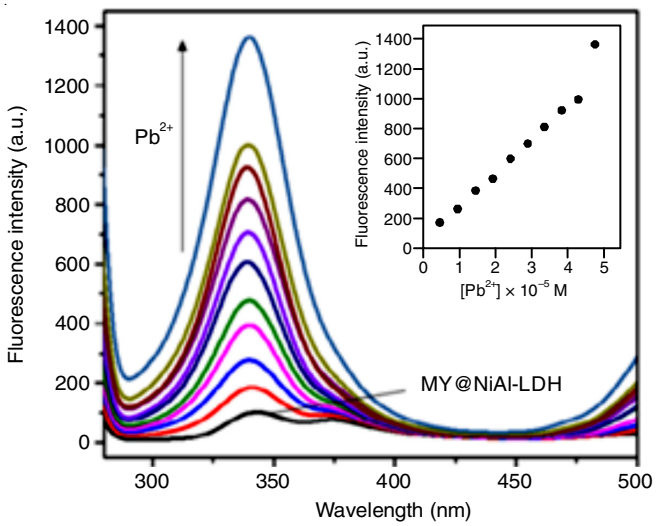

Fig. 9. Plot of fluorescence intensity of MY@NiAl-LDH in CH_3OH/PBS buffer (1:1, pH = 7.4) on the addition of aqueous solution of Pb^{2+} (10^{-3} M) (0-100 µL). (λ_{ex} = 275 nm, λ_{max} = 344 nm). The inset shows the plot of fluorescence intensity as a function of Pb^{2+} concentration

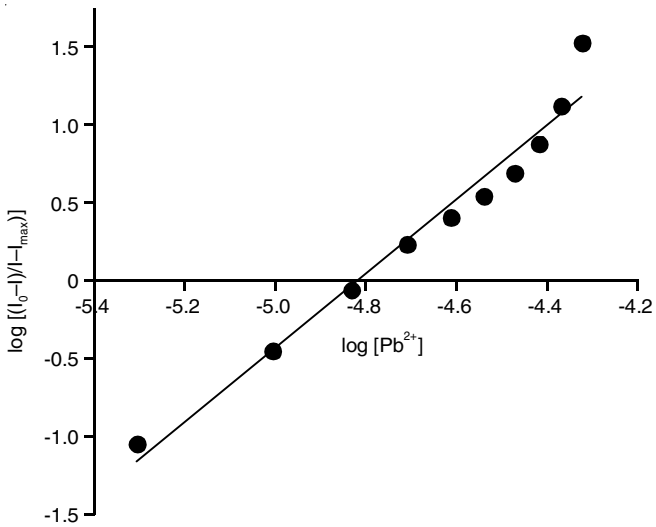

Fig. 10. Plot of log $[(I_0\text{-}I)/(I\text{-}I_{max})]$ *versus* log $[Pb^{2+}]$ of MY@NiAl-LDH

TABLE-1
LIMIT OF DETECTION (LOD) OF DIFFERENT FLUORESCENT SENSOR FOR Pb^{2+} ION

Probe	Limit of detection	Ref.
GO/G-quadruplex@acridine orange dye	3 nM	[22]
GO/AgNPs nanocomposites	50 nm	[23]
Xylenol orange functionalized CdSe/CdS quantum dots	0.2 µM	[24]
Glutathione-capped Mn-doped ZnS QDs@LDH	0.93 µM	[25]
Metanil yellow@NiAl-LDH	0.405 nM	This work

gradually increases whereas the peak at 275 nm showed a slight blue shift to 260 nm with enhancement in absorbance value. Fig. 11a depicts the effect of addition of Pb^{2+} ion on the UV-Vis spectrum of MY@NiAl-LDH in CH_3OH/PBS buffer. To deter-mine the binding stoichiometry, plot of log $[(A_0\text{-}A)/(A\text{-}A_{max})]$ *vs.* log $[Pb^{2+}]$ is shown in Fig. 11b, where A_0 is the absorbance of MY@NiAl-LDH in absence Pb^{2+}; A is the absorbance of MY@NiAl-LDH at different added concentration of Pb^{2+} and A_{max} is the highest absorbance value of MY@NiAl-LDH on adding one equivalent of Pb^{2+}. The slope of the graph was found to be 1.112, hence confirming a 1:1 interaction of MY@NiAl-LDH with Pb^{2+}.

Interference study: The possibility of interference by other metal ions on the selective determination of Pb^{2+} by MY@NiAl-LDH was studied by recording the fluorescence spectra of MY@NiAl-LDH in the presence of one equivalent of Pb^{2+} and other metal ion such as Na^+, K^+, Ca^{2+}, Cu^{2+}, Hg^{2+}, Cd^{2+}, Zn^{2+}, Al^{3+}, Co^{2+}, Fe^{2+}, Fe^{3+} and Ni^{2+}. Fig. 12 depicts in the form of a bar diagram that only Pb^{2+} could increase the fluorescent intensity of MY@NiAl-LDH even in the presence of one equivalent of other metal ions. The red bar in the bar diagram represents the fluorescence intensity of MY@NiAl-LDH in presence of the other metal ions while the blue bar indicates the fluorescence intensity of MY@NiAl-LDH with Pb^{2+} ions in presence of other metal ions.

Reversibility study: The criterion of reversible binding of sensor MY@NiAl-LDH towards Pb^{2+} was checked through titration with $EDTA^{2-}$. When the metal ion chelator Na_2EDTA

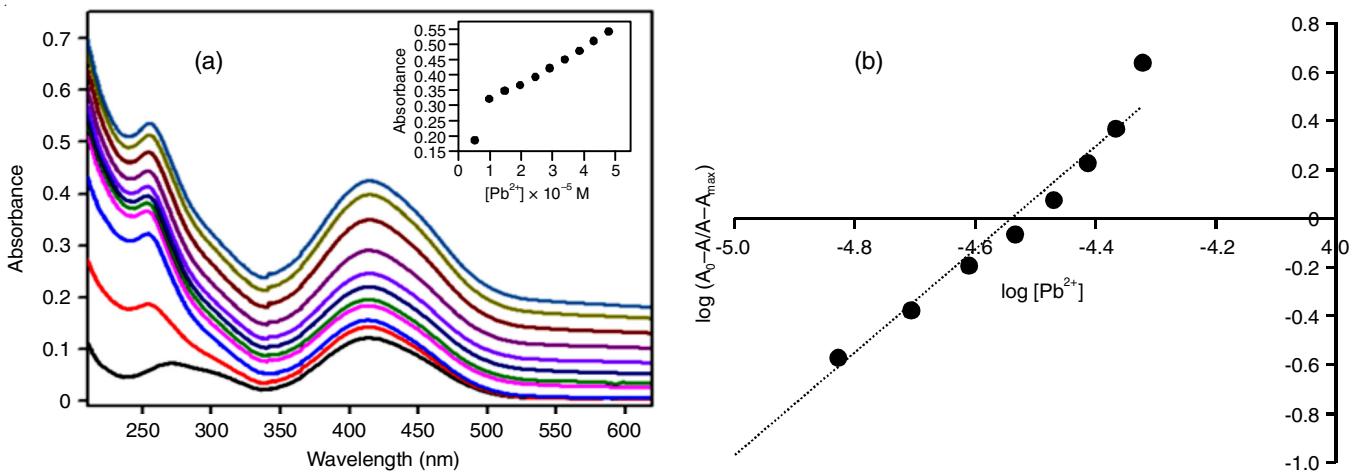

Fig. 11. (a) Plot of UV-Vis spectra of MY@NiAl-LDH in CH_3OH/PBS buffer (1:1, pH = 7.4) on addition of aqueous solution of Pb^{2+}. The inset shows the plot of concentration *vs.* absorbance and (b) Plot of log $[(A_0\text{-}A)/(A\text{-}A_{max})]$ *vs.* log $[Pb^{2+}]$ of MY@NiAl-LDH

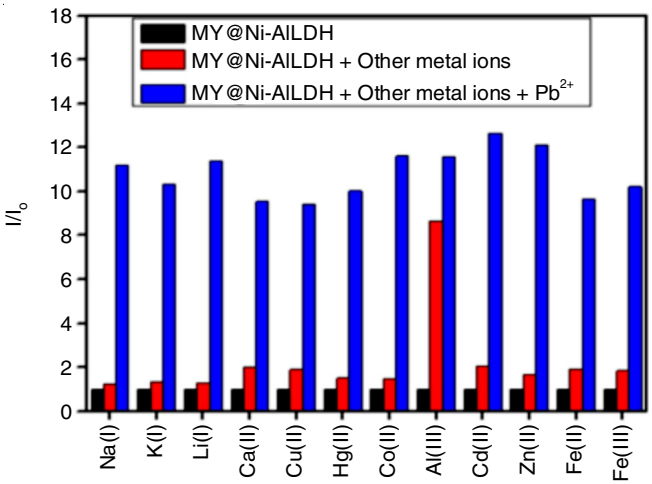

Fig. 12. Selectivity of MY@NiAl-LDH towards Pb^{2+} in the presence of other metal ions

was added to a 1:1 solution of MY@NiAl-LDH and Pb^{2+}, the fluorescence intensity was found to decline with the gradual addition of $EDTA^{2-}$ until it reached the intensity of MY@NiAl-LDH. Fig. 13 shows the reversible binding of MY@NiAl-LDH with Pb^{2+}, which indicates that $EDTA^{2-}$ chelates away the metal from its complex with the sensor.

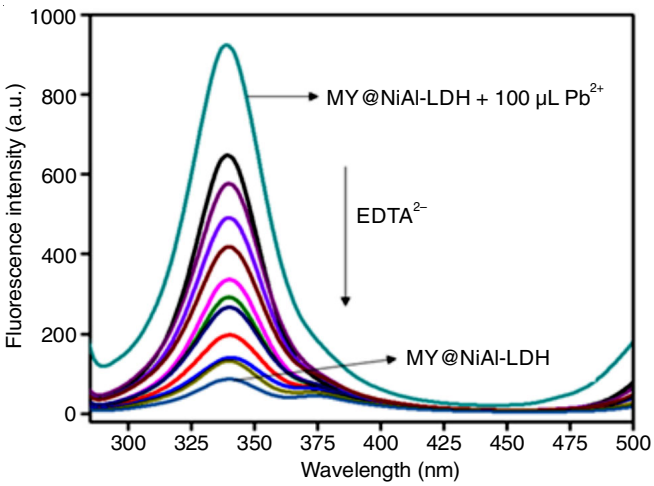

Fig. 13. Fluorescence intensity curve of reversible behaviour of MY@NiAl-LDH

Probable mechanism: Upon titrating with Pb^{2+} ions, the metal ion complexes with the azo dye loaded onto the outer surface or interlayer space of the LDH. However, the complexation of the metal ion with metanil yellow dye may be difficult within the deep interlayer space of the NiAl-LDH due to difficulty in diffusion of Pb^{2+} ions within the hydrophobic interlayer space. Therefore, complex formation of Pb^{2+} is more favourable with the azo dye adsorbed on the external surface of NiAl-LDH. Furthermore, the increment in the fluorescence intensity of the sensor upon its interaction with Pb^{2+} ion can be explained on the basis of the thermodynamically favoured photo induced electron transfer (PET) mechanism. The intercalated dye consists of the chromophoric N=N group, the NH group and the O atom from the electron withdrawing $PhSO^{3-}$ group. Upon irradiation with 275 nm, electron transfer takes place from the electron rich group to the deficit group, thereby resulting in PET process. However, upon titration with Pb^{2+} ion, it coordinates with the N-atom of the azo linkage and O-atom of the sulphonate group thereby snapping the PET process and this result in the enhancement of fluorescence intensity.

MY@NiAl-LDH as electrochemical sensor for Al^{3+}: A three-electrode electrochemical system consisting of modified platinum electrode (working electrode), Ag-AgCl (reference electrode) and Pt wire (auxiliary electrode) was used to study the behaviour of MY@NiAl-LDH towards its detection of Al^{3+} in presence of other metal ions. The platinum electrode was cleaned prior to modification as per reported [26]. A 10 mg of the prepared sensor was taken in 1 mL of acetonitrile containing a few drops of styrene and then 2 µL of this solution was drop cast onto the surface of cleaned Pt electrode. The process was repeated three times and the electrodes were allowed to dry in the nitrogen environment to carry out the electrochemical experiments. The cyclic voltammetry studies were performed on the modified electrode in order to determine its sensing capability. The successful modification of the Pt electrode namely, MY@NiAl-LDH/Pt electrode is represented in its cyclic voltammogram (CV) and chronocoulometry (CC) signal (Fig. 14). From these plots, the total surface coverage of the electrodes has been calculated employing the equation $Ip = n^2F^2A\Gamma\nu/4RT$ [27]. The total surface coverage for the modified electrode was found to be 2.38×10^{-3} mol cm^{-2}, which was 137.4% larger than the bare Pt electrode. Hence, this justifies the enhanced electrochemical sensitivity of the modified Pt electrode compared to the bare Pt electrode due to presence of an electroactive compound.

As depicted in Fig. 15a, the cyclic voltammogram response of MY@NiAl-LDH/Pt electrode shows a cathodic peak at -0.881 V and an anodic peak at -0.702 V in presence of an added concentration of Al^{3+}. The peak separation was calculated to be 0.179 V and $E_{1/2}$ was found to be -0.791 V, respectively. Fig. 15b depicts the CV response of MY@NiAl-LDH/Pt in PBS at different added concentrations of Al^{3+}. With increasing concentration of Al^{3+} ions, the reduction peak gradually increases while the oxidation peak is shifted to the left side. In this case, Al^{3+} ions underwent strong coordination by complexing with the hard site *i.e.* N and O atom in the sensor. The rise of a new cathodic peak can be assigned to the electron transfer between the complex formed with the sensor and Al^{3+} ions in solution. The shift in the anodic potential can be attributed to the involvement of azo group in complexation followed by its consequent stabilization in the ring making it less available for reduction [28]. The inset of Fig. 15b shows a linear plot of the cathodic peak current with respect to concentration of Al^{3+} ion with a good linear correlation of $R^2 = 0.9936$. The limit of detection of Al^{3+} ions from the cyclic voltammogram data was calculated as per the formula: $3\sigma/K$ [29], where σ = standard deviation, K = slope obtained from the plot of cathodic current *vs.* concentration (Fig. 15b, inset). The LOD was obtained to be 1.57 nM.

The effect of an increase in scan rate on the modified electrode is shown in Fig. 16a. As the scan rate is increased from 10 to 100 mV s^{-1}, the cathodic and anodic peak current

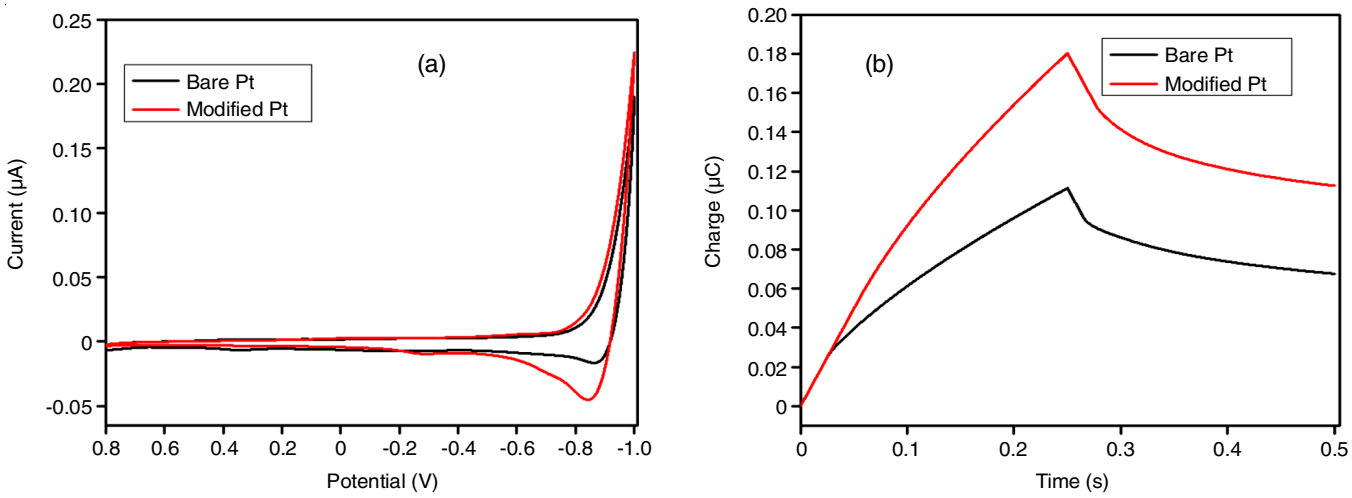

Fig. 14. (a) Cyclic voltammogram and (b) Chronocoulometry response of bare Pt electrode and MY@NiAl-LDH/Pt

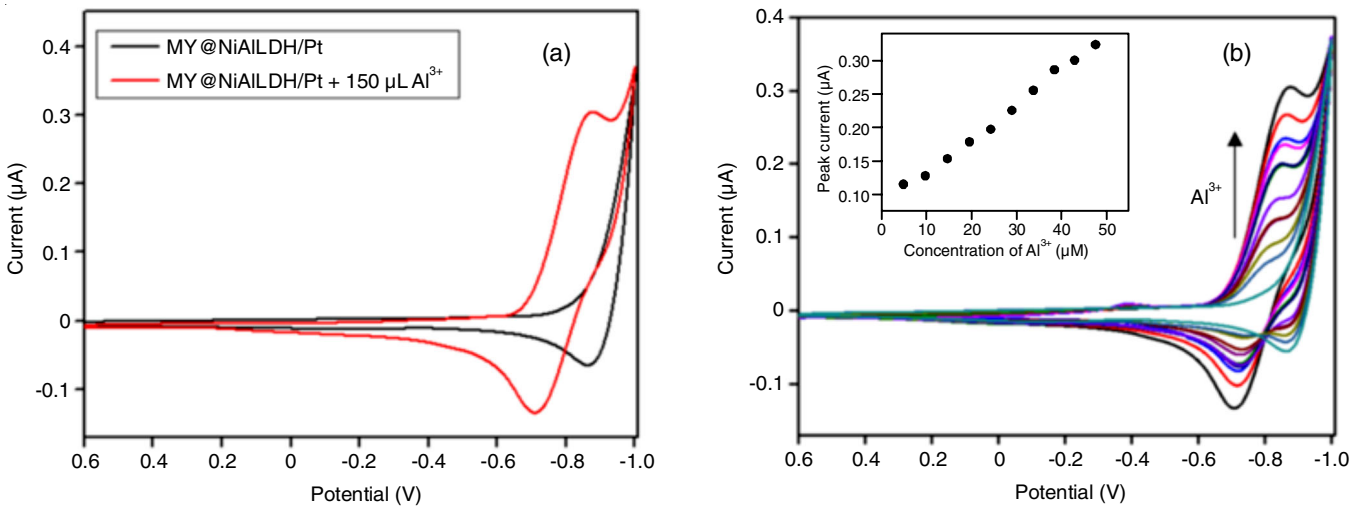

Fig. 15. (a) Cyclic voltammogram of MY@NiAl-LDH/Pt in PBS (pH = 7.4) in absence (black line) and presence (red line) of 150 μL of Al^{3+} ion. (RE: Ag-AgCl, SE: 0.1 M KCl, scan rate: 10 mVs^{-1}) and (b) Cyclic voltammogram of MY@NiAl-LDH/Pt in PBS (pH = 7.4) upon addition of different concentration of Al^{3+} ion. The inset shows the plot of peak current *vs.* Al^{3+} concentration

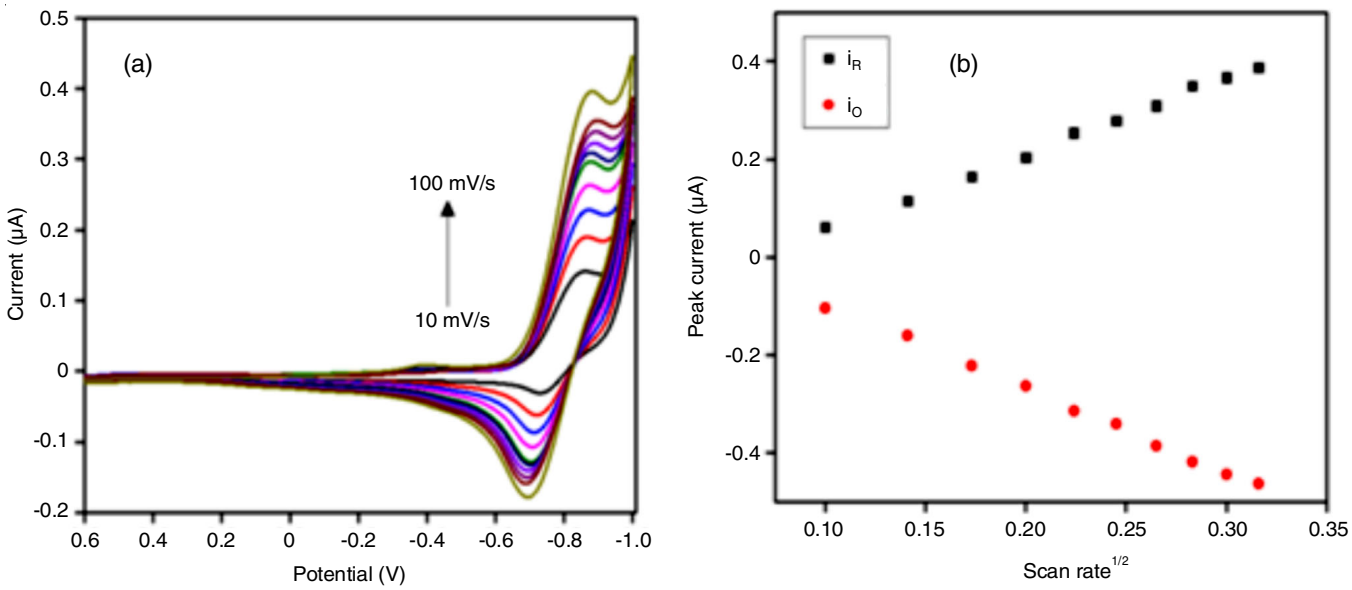

Fig. 16. (a) Cyclic voltammogram of MY@NiAl-LDH/Pt with Al^{3+} (50 μL) in PBS (pH = 7.4) at different scan rates (RE: Ag-AgCl, SE: 0.1 M KCl), (b) Plot of cathodic and anodic peak currents *vs.* square root scan rate ($n^{1/2}$)

increases gradually. The positions of the cathodic and anodic current do not undergo any major shift of peaks with increasing scan rates. This illustrates the reversible nature of detection, which is kinetically controlled by diffusion of the analyte on the surface of MY@NiAl-LDH/Pt electrode. The plot of oxidation and reduction peak current *vs.* square root of scan rate demonstrates a linear graph (Fig. 16b), which is also described by the Randle-Sevcik equation [30]. The correlation coefficient (R^2) values for the oxidation and reduction wave were observed as 0.9965 and 0.9921, respectively.

Interference from other ions: The cyclic voltammetry were conducted to study the selectivity of MY@ NiAl-LDH/Pt towards the detection of Al^{3+} ion in presence of other metal ions such as Na^+, K^+, Zn^{2+}, Hg^{2+}, Fe^{2+}, Pb^{2+}, Mg^{2+}, Ni^{2+}, Ca^{2+}. The CV responses showed that the other metal ions did not show any significant peak and the presence of the metal ions did not interfere with the determination of Al^{3+} by the modified electrode. Furthermore, in presence of other metal ions, the CV response for Al^{3+} ion showed a cathodic peak at -0.608 V and an anodic peak at -0.424 V, respectively (Fig. 17).

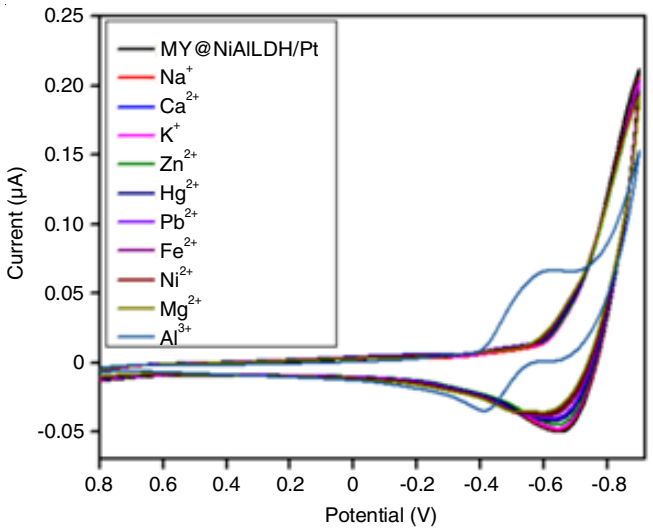

Fig. 17. Cyclic voltammogram of MY@NiAl-LDH/Pt in PBS (pH = 7.4) for Al^{3+} ions in presence of other metal ions

Conclusion

In summary, a layered double hydroxide of nickel and aluminium (NiAl-LDH) was successfully synthesized by hydrothermal process. Successful inclusion of the metanil yellow dye into the LDH allowed for the use of the probe to detect Pb^{2+} and Al^{3+} ions exclusively using fluorescence spectroscopy and electrochemical measurements. The sensor MY@NiAl-LDH shows an excellent turn-on fluorescence signal for Pb^{2+} ions with limit of detection (LOD) calculated to be 0.405 nM. Platinum electrode modified with the sensor selectively detects Al^{3+} ions with distinctively separated cathodic and anodic peaks and having low LOD value of 1.57 nM. The detection of the metal ions were free from any sort of interferences. The developed method demonstrated excellent sensitivity, selectivity, reversibility and simplicity and expected that dye-intercalated LDHs have broad promising applications in the detection of biological and environmentally important ions.

ACKNOWLEDGEMENTS

The authors thank SAIF, Gauhati University for providing the instrumental facilities and Dr. Sangeeta Agarwal, Cotton University, Gauhati, India for conducting the UV-VIS/diffuse reflectance analysis.

CONFLICT OF INTEREST

The authors declare that there is no conflict of interests regarding the publication of this article.

REFERENCES

1. K.H. Vardhan, P.S. Kumar and R.C. Panda, *J. Mol. Liq.*, **290**, 111197 (2019); https://doi.org/10.1016/j.molliq.2019.111197
2. V. Shukla, P. Shukla and A. Tiwari, *Indian J. Med. Special.*, **9**, 146 (2018); https://doi.org/10.1016/j.injms.2018.04.003
3. D.R. Wallace and A. Buha Djordjevic, *Curr. Opin. Toxicol.*, **19**, 72 (2020); https://doi.org/10.1016/j.cotox.2020.01.001
4. Z. Es'haghi, M. Khalili, A. Khazaeifar and G.H. Rounaghi, *Electrochim. Acta*, **56**, 3139 (2011); https://doi.org/10.1016/j.electacta.2011.01.064
5. S.M. Supian, T.L. Ling, L.Y. Heng and K.F. Chong, *Anal. Methods*, **5**, 2602 (2013); https://doi.org/10.1039/c3ay40238j
6. T.P. Flaten, *Brain Res. Bull.*, **55**, 187 (2001); https://doi.org/10.1016/S0361-9230(01)00459-2
7. Z.C. Liao, Z.Y. Yang, Y. Li, B.D. Wang and Q.X. Zhou, *Dyes Pigments*, **97**, 124 (2013); https://doi.org/10.1016/j.dyepig.2012.12.017
8. R.J. Cassella, O.I.B. Magalhaes, M.T. Couto, E.L.S. Lima, M.A.F.S. Neves and F.M.B. Coutinho, *Talanta*, **67**, 121 (2005); https://doi.org/10.1016/j.talanta.2005.02.019
9. S.L.C. Ferreira, A.S. Queiroz, M.S. Fernandes and H.C. dos Santos, *Spectrochim. Acta B At. Spectrosc.*, **57**, 1939 (2002); https://doi.org/10.1016/S0584-8547(02)00160-X
10. S. Knezevic, R. Milacic and M. Veber, *Fresenius J. Anal. Chem.*, **362**, 162 (1998); https://doi.org/10.1007/s002160051050
11. J. Kumar, M. Sarma, P. Phukan and D.K. Das, *Dalton Trans.*, **44**, 4576 (2015); https://doi.org/10.1039/C4DT03932G
12. M. Gao and B.Z. Tang, *ACS Sens.*, **2**, 1382 (2017); https://doi.org/10.1021/acssensors.7b00551
13. D. Scarpellini, C. Falconi, P. Gaudio, A. Mattoccia, P.G. Medaglia, A. Orsini, R. Pizzoferrato and M. Richetta, *Microelectron. Eng.*, **126**, 129 (2014); https://doi.org/10.1016/j.mee.2014.07.007
14. F.J. Quites, J.C. Germino and T.D.Z. Atvars, *Colloids Surf. A Physicochem. Eng. Asp.*, **459**, 194 (2014); https://doi.org/10.1016/j.colsurfa.2014.07.009
15. R. Amini, E. Rahimpour and A. Jouyban, *Anal. Chim. Acta*, **1117**, 9 (2020); https://doi.org/10.1016/j.aca.2020.04.001
16. N. Senda, I. Fujiwara and Y. Murakami, *Appl. Clay Sci.*, **183**, 105310 (2019); https://doi.org/10.1016/j.clay.2019.105310
17. J. Dong, Q. Fang, H. He, Y. Zhang, J. Xu and Y. Sun, *Mikrochim. Acta*, **182**, 653 (2015); https://doi.org/10.1007/s00604-014-1369-4
18. M. Liu, G. Lv, L. Mei, Y. Wei, J. Liu, Z. Li and L. Liao, *Sci. Rep.*, **7**, 13414 (2017); https://doi.org/10.1038/s41598-017-13779-1
19. H. Saikia and J.N. Ganguli, *Asian J. Chem.*, **24**, 5909 (2012).

20. N. Bhuvanesh, S. Suresh, K. Velmurugan, A. Thamilselvan and R. Nandhakumar, *J. Photochem. Photobiol. Chem.*, **386**, 112103 (2020); https://doi.org/10.1016/j.jphotochem.2019.112103
21. X. Lai, R. Wang, J. Li, G. Qiu and J.B. Liu, *RSC Adv.*, **9**, 22053 (2019); https://doi.org/10.1039/C9RA03776D
22. Y. Bai, L. Zhao, Z. Chen, H. Wang and F. Feng, *Anal. Methods*, **6**, 8120 (2014); https://doi.org/10.1039/C4AY01389A
23. P.O. Patil, G.R. Pandey, A.G. Patil, V.B. Borse, P.K. Deshmukh, D.R. Patil, R.S. Tade, S.N. Nangare, Z.G. Khan, A.M. Patil, M.P. More, M. Veerapandian and S.B. Bari, *Biosens. Bioelectron.*, **139**, 111324 (2019); https://doi.org/10.1016/j.bios.2019.111324
24. Q. Zhao, X. Rong, H. Ma and G. Tao, *Talanta*, **114**, 110 (2013a); https://doi.org/10.1016/j.talanta.2013.04.016
25. J. Liu, G. Lv, W. Gu, Z. Li, A. Tang and L. Mei, *J. Mater. Chem. C Mater. Opt. Electron. Devices*, **5**, 5024 (2017); https://doi.org/10.1039/C7TC00935F
26. J. Rajbongshi, D.K. Das and S. Mazumdar, *Electrochim. Acta*, **55**, 4174 (2010); https://doi.org/10.1016/j.electacta.2010.02.045
27. S. Liu, H.L. Li, M. Jiang and P. Li, *J. Electroanal. Chem.*, **426**, 27 (1997); https://doi.org/10.1016/S0022-0728(97)00021-1
28. O. Abollino, M. Aceto, C. Sarzanini and E. Mentasti, *Electroanalysis*, **11**, 870 (1999); https://doi.org/10.1002/(SICI)1521-4109(199908)11:12<870::AID-ELAN870>3.0.CO;2-L
29. R.N. Hegde, B.E. Kumara Swamy, N.P. Shetti and S.T. Nandibewoor, *J. Electroanal. Chem.*, **635**, 51 (2009); https://doi.org/10.1016/j.jelechem.2009.08.004
30. J.K. Shashikumara and B.E. Kumara Swamy, *Sens. Int.*, **1**, 100008 (2017); https://doi.org/10.1016/j.sintl.2020.100008